ACS APPLIED MATERIALS & INTERFACES

Research Article

www.acsami.org

Poly(3-hexylthiophene) Nanotubes with Tunable Aspect Ratios and Charge Transport Properties

Long-Biao Huang,[†] Zong-Xiang Xu,[‡] Xianfeng Chen,[†] Wei Tian,[§] Su-Ting Han,[†] Ye Zhou,[†] Jia-Ju Xu,[†] Xiong-Bo Yang,[†] and Vellaisamy A. L. Roy*,[†]

[†]Center of Super-Diamond and Advanced Films (COSDAF) and Department of Physics and Materials Science, City University of Hong Kong, Hong Kong, Hong Kong SAR

[‡]Department of Chemistry, South University of Science and Technology of China, Shen Zhen, Guangdong 518000, P. R. China

[§]The Key Laboratory of Space Applied Physics and Chemistry, Ministry of Education and Shaanxi Key Laboratory of Macromolecular Science and Technology, School of Science, Northwestern Polytechnical University, Xi'an, Shaanxi 710072, P. R. China

S *Supporting Information*

ABSTRACT: Regioregular poly(3-hexylthiophene) (RR-P3HT) nanotubes (200 nm in diameter) with tunable aspect ratios from 25 to 300 were prepared using a polymer melt wetting technique. Aspect-ratio tunability was achieved by controlling the wetting behavior of RR-P3HT melts in a template. The crystallinity and chain orientation of RR-P3HT were studied by grazing incidence X-ray diffraction, wide-angle X-ray diffraction, and polarized photoluminescence spectroscopy. Results suggest that RR-P3HT chains in the lamellar structure prefer to be perpendicular to the axis of the RR-P3HT nanotubes, forming a face-on conformation in the RR-P3HT nanotubes that leads to increased carrier mobility of RR-P3HT. Field-effect transistors were fabricated based on a single RR-P3HT nanotube and showed a carrier mobility of 0.14 ± 0.02 $cm^2/V{\cdot}s$.

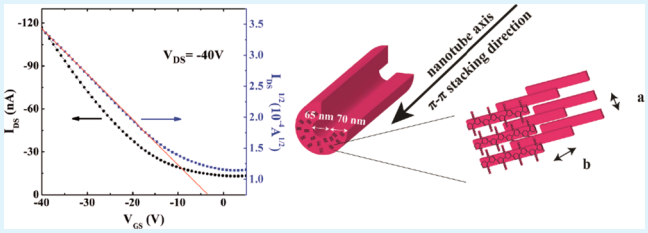

KEYWORDS: *RR-P3HT, AAO, nanotube array, tunable aspect ratios, field-effect transistor, charge transport properties*

INTRODUCTION

1-Dimensional (1D) organic/inorganic semiconductor nanowires are promising building blocks attracting huge attention from the academia and industries. These nanowires have various electronic and optoelectronic applications including field-effect transistors (FETs),[1,2] light-emitting diodes (LEDs),[3] solar cells,[4−6] nanoscale lasers,[7] memory devices,[8] photo switches,[9] ion battery,[4,10,11] and vapor sensor.[12,13] Compared with the 1D nanostructure of inorganic semiconductors and metals, 1D-conjugated polymer semiconductors need more understanding in order to get excellent tunability over size, crystal structure, and composition.[14] Currently, there are three methods that can be used to fabricate 1D conjugated polymer semiconductors, namely the following: (i) solution synthesis,[12] (ii) supramolecular self-assembly in dilute solutions or at solvent/substrate interface such as spin-coating[15−19] and drop-casting,[20,21] and (iii) electrospinning[22,23] under high voltage (e.g., blends of RR-P3HT and poly ε-caprolactone[24,25]). However, to keep the tunability of dimensions and suitable crystallinity by using these three processes is a challenge.

Here, we suggest a simple technique for the preparation of a 1D conjugated polymer semiconductor nanostructure with tunable aspect ratios and suitable crystallinity. Steinhart[26] et al. have pioneered a polymer melt wetting technique in preparing 1D nanowires/nanotubes. Several studies[11,16,27−30] utilized the technology to create different polymer nanotubes/nanowires, and these studies revealed that polymer crystallization of the as-prepared 1D nanowires/nanotubes lead to different structures from the bulk polymer. The perpendicular orientation of polyvinylidene fluoride (PVDF) chains with respect to PVDF nanotubes has been reported[27,31] for syndiotactic polystyrene[11,32,33] and polyethylene.[16] This anisotropic structure of polymer chains strongly influences their physical properties including optical, electronic, mechanical, and semiconducting[27] properties. However, only a few reports[34,35] have mentioned the formation of anisotropic nanorod arrays and nanopillars of semiconductor polymers using such techniques. Furthermore, these reports did not analyze the crystal orientation, which provides crucial information on the potential application in organic transistors and solar cells.

In this study, a polymer melt wetting technique was used to prepare anisotropic 1D nanotubes of regioregular poly(3-hexylthiophene) (RR-P3HT) with tunable aspect ratios. Crystallinity and charge-transport properties were analyzed. RR-P3HT has aroused great attention and is widely used in organic FETs and polymer solar cells because of its interesting optoelectronic properties, such as high charge-carrier mobility (10^{-2} $cm^2/V{\cdot}s$ to 10^{-3} $cm^2/V{\cdot}s$), crystal structure ((100) and

Received: December 5, 2012
Accepted: July 11, 2014
Published: July 11, 2014

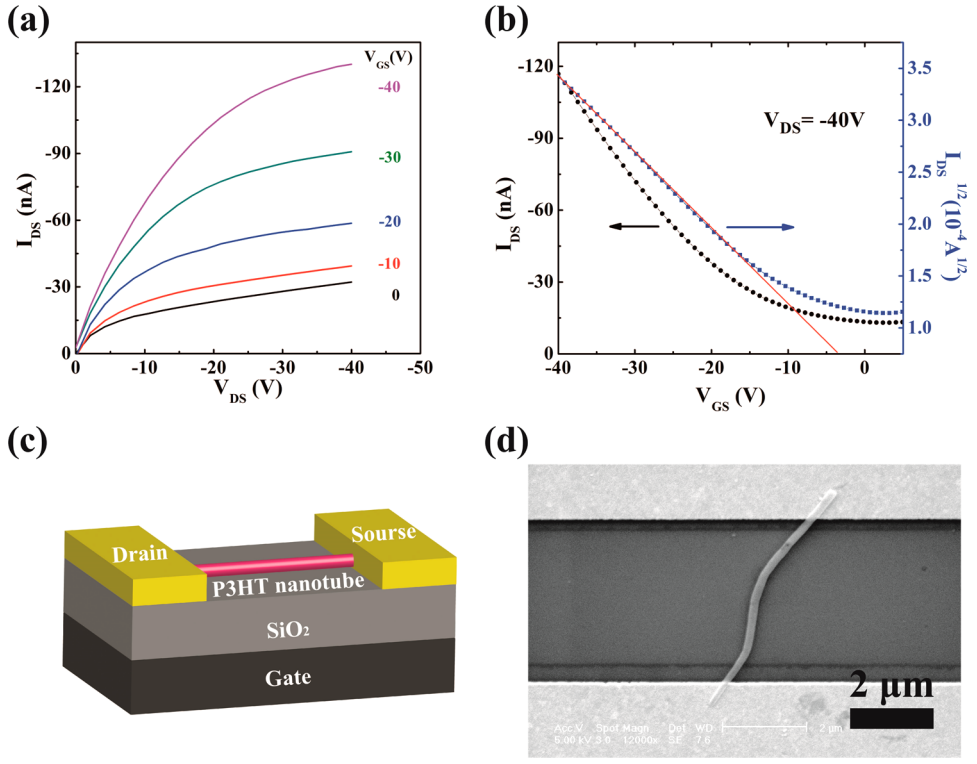

Figure 1. (a) Output and (b) transfer characteristics of single RR-P3HT nanotube transistors; (c) schematic of single nanotube FET device; and (d) SEM image of single nanotube device.

(010) reflection for lamella layer structure), and $\pi-\pi$ stacking.[36] Optoelectronic devices largely depend on the crystal orientation of polymer semiconductors such as "edge-on" and "face-on" in which the thiophene ring is perpendicular and parallel to the substrate,[36] respectively. As previously reported[37,38] RR-P3HT was hot-pressed into a ~200 μm film under nitrogen atmosphere for the fabrication of the RR-P3HT nanotubes in a hard-template polymer melt wetting process. Subsequently, a systematic study on the aspect-ratio control of the RR-P3HT nanotubes was performed. Ordered microcrystalline and amorphous domains in semiconducting conjugated polymers have an important role in the performance of organic nanodevices,[39] and, therefore, the intrinsic structures of the RR-P3HT nanotubes were investigated using grazing incidence X-ray diffraction (GIXRD), wide-angle X-ray diffraction (WAXD), and polarized photoluminescence spectroscopy. Furthermore, charge carrier mobility was measured using FET configuration.

EXPERIMENTAL SECTION

Materials. Regioregular poly(3-hexylthiophene) (RR-P3HT, Mn = 54 000 to 75 000, $M_w/M_n \leq 2.5$, >98% head-to-tail regioregular), sodium hydroxide, absolute ethanol, isopropyl alcohol, and chloroform were purchased from Sigma-Aldrich and used without further purification. Anodized alumina oxide (AAO) templates were purchased from Whatman (U.K.) with a through-hole channel diameter of ~200 nm and channel length of about 60 μm.

Differential Scanning Calorimetry (DSC) of RR-P3HT. The thermal properties of bulk RR-P3HT were investigated using a PerkinElmer DSC7 with a refrigerated cooler. Before measuring RR-P3HT, indium and zinc were used to calibrate the instrument. The RR-P3HT sample (~8 mg) was heated to 300 °C and held for 10 min to release the thermal history followed by cooling to 30 °C and then reheated to 300 °C. The heating and cooling were controlled at a rate of 10 °C/min.

Preparation of RR-P3HT Nanotubes. First, RR-P3HT films, with thickness of ~200 μm, were prepared by hot pressing at 220 °C in nitrogen atmosphere and then were placed on the surface of AAO templates that had been sequentially rinsed for an hour with ethanol, isopropyl alcohol, and chloroform. Second, the assembled samples with RR-P3HT films on AAO templates were heated in an oven (Delta 9023 with temperature resolution of 0.1 °C, Delta Design a Cohu Company). The heating temperature was sequentially set at 200, 210, 220, 230, 240, and 250 °C, following the thermal properties of RR-P3HT. Third, after 10 min of maintaining at the set temperature, RR-P3HT melted to wet into the nanochannels of AAO. Then, the assembled samples were cooled to ambient temperature at a rate of 10−15 °C/min. Fourth, the RR-P3HT nanotubes were released from the AAO templates using sodium hydroxide solution (5 wt %), rinsed with deionized water and absolute ethanol for several times, and then dried in a vacuum oven set at 30 °C for 24 h. Last, the prepared RR-P3HT nanotubes were removed using a blade and were dispersed in absolute ethanol for device fabrication.

Characterization of RR-P3HT Nanotubes. The RR-P3HT film with nanotubes on the surface was characterized using an environmental scanning electron microscopy (SEM) system (FEI/Philips XL30 Esem-FEG). Meanwhile, a transmission electron microscopy (TEM) system (Philips Technai 12) was used to check the nanotubes. For the cross-section image, the samples were kept in liquid nitrogen for an hour and then were broken into pieces. A field-emission SEM (FESEM) instrument (JEOL JSM-6335F) was used to check the inner diameter and wall thickness of the RR-P3HT nanotubes, which were removed using a sharp blade in liquid nitrogen.

For the investigation of the crystal orientation of the RR-P3HT nanotubes located inside the AAO templates, GIXRD and WAXD (Rigaku SmartLab) experiments were performed. The grazing X-ray incident angle was fixed at 0.5° to the surface plane of samples. The detector scans were performed from 3° to 30°. The surface of the AAO template with the RR-P3HT nanotubes was kept perpendicular to the plane defined by the grazing incident beam and detector.[27,31,40,41] In this setup, the Bragg reflection was mainly relative to the crystal planes that are parallel to the AAO template.[33]

The P3HT nanotubes fabricated at 210 °C were used to measure GIXRD. The P3HT nanotube strands on the amorphous silicon plate and solution-processed P3HT film (10 mg/mL in dichlorobenzene at 1000 rpm for 30 s) were also measured.

Polarized photoluminescence measurements (emission mode) were carried out using a 490 nm excitation wavelength with a Spex Fluorolog-3 spectrofluorometer system (Horiba Jobin Yvon) having a 450 W xenon lamp as the steady-state excitation source. Polarized light was irradiated on the aligned RR-P3HT nanotubes, which were prepared by cutting cross-sectionally in liquid nitrogen. The polarized emission was collected at a perpendicular direction with respect to the excitation light. The plane defined by excitation and emission lights was perpendicular to the RR-P3HT nanotube axis. The RR-P3HT nanotube arrays fabricated at 210 °C and removed from the AAO template were measured.

Preparation and Characterization of Single RR-P3HT Nanotube Field-Effect Transistors. A typical top-contact/bottom-gate configuration was selected for single RR-P3HT nanotube FETs. The as-fabricated RR-P3HT nanotubes were dispersed in ethanol. Then, the diluted P3HT nanotubes/ethanol solution was dropped on the surface of a 300 nm thick SiO_2/Si wafer to form individually dispersed nanotubes, where SiO_2 and Si served as the dielectric and gate electrodes, respectively. After drying in an oven, Cr (20 nm) and Au (60 nm) were deposited on a single RR-P3HT nanotube through a shadow mask (metal wire with diameter of 5 μm) using sputtering to form the source and drain electrodes. To reduce the damage caused by the deposition of metal on the RR-P3HT nanotubes, the deposition rate of the electrode was set at 0.03 nm/s using Temescal CV-8. The output and transfer characteristics of the devices were measured using a probe station connected to a semiconductor parameter analyzer (Keithley 4200) inside a nitrogen glovebox (Mbraun).

RESULTS AND DISCUSSTION

FETs based on single RR-P3HT nanotubes were fabricated and measured to analyze the charge-transport properties of the RR-P3HT nanotubes. In this work, the RR-P3HT nanotubes with a length of ~6 μm fabricated at 210 °C for 10 min were used for the FET devices. Figure 1 presents the output and transfer characteristics of a single RR-P3HT nanotube transistor. The schematic of the FET device and the SEM image of the device are shown in Figures 1c and 1d, respectively. The FET device shows typical p-type transistor behavior where the negative drain-source current increases with increasing negative gate voltages. The field-effect mobility was calculated at the saturation regime using the equation $I_{ds} = WC_i\mu/2L(V_{gs}-V_{th})^2$, where I_{ds} is the drain-source current through the RR-P3HT nanotube, V_{gs} and V_{th} are the gate voltage and threshold voltage, respectively, and C_i is the capacitance of the 300 nm thick SiO_2 gate dielectric. For mobility calculations, W and L are defined as the width of the nanotube (200 nm) and the length (5 μm) across the source-drain electrodes, respectively. The average W/L ratio of the RR-P3HT nanotubes between two gold electrodes was about 0.04 (Figure 1d). More than 20 FET devices were tested, and an average mobility of 0.14 ± 0.02 $cm^2/V{\cdot}s$ was obtained and shown in Figure S1. The output and transfer curves are shown in Figures 1a and 1b. Although our devices were fabricated without surface modification of the dielectric layer, the obtained carrier mobility was higher than that of devices made up of RR-P3HT nanofibers from electrospinning[42] and similar to the surface of thin-film devices modified with octadecyltrichlorosilane[43] on a dielectric layer. The results showed that semiconductor polymer nanowires/nanotubes fabricated using a polymer melt wetting technique possess better charge-transport properties. The improved mobility could be attributed to the chain orientation or crystallinity of RR-P3HT.

As mentioned above, the chain orientation or crystallinity of semiconductor polymers substantially determines the optoelectronic properties[44] because of the differences in the charge-transport mechanism of conjugated polymers. For example, the direction of $\pi-\pi$ stacking of the thiophene ring would determine the carrier mobility of the RR-P3HT nanotubes. For a solution-processed RR-P3HT film, the FET device with the thiophene ring perpendicular to the substrate has higher carrier mobility than that with the thiophene ring parallel to the substrate.[20] In our case, the high carrier mobility of the RR-P3HT nanotubes may imply that the thiophene ring was perpendicular to the nanotube axis, whose inner structure is schematically shown in Figure 2. The FESEM images of the

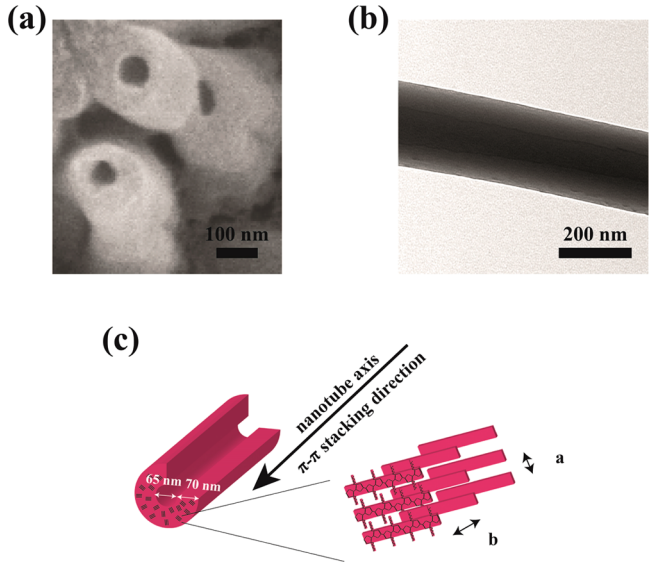

Figure 2. (a) FESEM image of the RR-P3HT nanotubes; (b) TEM image of the RR-P3HT nanotube; and (c) schematic of the inner structure of a single RR-P3HT nanotube.

RR-P3HT nanotubes prepared in liquid nitrogen using a sharp blade are shown in Figure 2a. The TEM image of the RR-P3HT nanotube is shown in Figure 2b. The results show that the inner diameter and wall thickness of the RR-P3HT nanotubes are about 65 and 70 nm, respectively. A proposed schematic of the inner structure of a single RR-P3HT nanotube is presented in Figure 2c. During the wetting process, the RR-P3HT chains are absorbed into the nanochannels by capillary force, and then nanotubes are formed with a diameter of around 200 nm with a 65 nm hollow hole. Lamellar structures of RR-P3HT are embedded into the 70 nm thick wall of the nanotubes. The $\pi-\pi$ stacking, formed by the thiophene ring of RR-P3HT, is perpendicular to the RR-P3HT nanotube axis, which causes the face-on conformation of the RR-P3HT lamella in the RR-P3HT nanotubes and leads to high carrier transport property.[45]

To confirm our hypothesis, GIXRD was used to investigate the chain orientation in the RR-P3HT nanotubes, including a solution-processed thin film for comparison. As shown in Figure 3a, three main edge-on-edge diffraction peaks, (100), (200), and (300), arising from the interdigitation of the hexyl groups were observed for the RR-P3HT nanotubes (red and black lines in Figure 3a). The large intensity of the (100) peak at a 2-theta value of 5.3° represents the edge-on conformation of the RR-P3HT crystal. The $\pi-\pi$ stacking diffraction peak

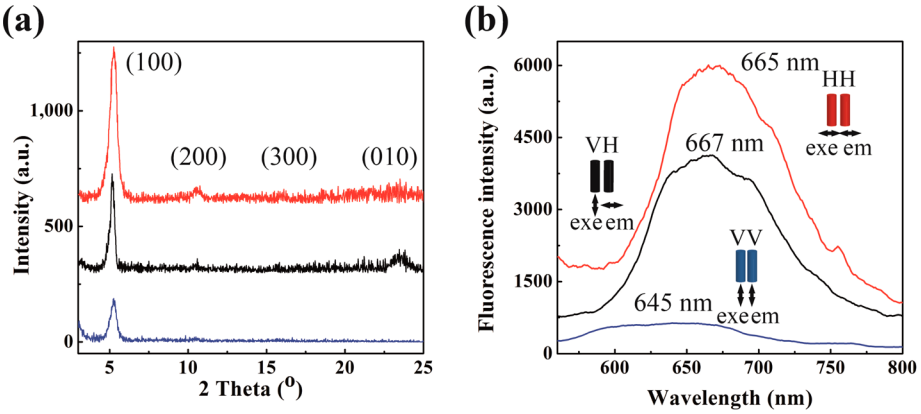

Figure 3. (a) GIXRD patterns of the RR-P3HT nanotubes fabricated in 10 min with a wetting temperature of 210 °C (red line for the RR-P3HT nanotube strands on an amorphous silicon, black line for the individual RR-P3HT nanotubes inside the templates, and blue line for a solution-processed RR-P3HT film; 10 mg/mL in dichlorobenzene with 1000 rpm and 30 s); (b) polarized photoluminescence of the RR-P3HT nanotubes (red line (I_{HH}) for polarized excitation and emission light collected perpendicular to the RR-P3HT nanotube axis, and black (I_{VH}) and blue lines (I_{VV}) for polarized emission light collected perpendicular and parallel with excitation light parallel to nanotube axis, respectively).

(010) originating from a face-on conformation of the RR-P3HT crystal is clearly visible at about 23° for the individual RR-P3HT nanotubes inside the templates and the RR-P3HT nanotube strands on an amorphous silicon. Meanwhile, the (010) diffraction peak for the solution-processed RR-P3HT thin film, which only exhibits (100) and (200) diffraction peaks (blue line in Figure 3a), is hard to find. The above-described GIXRD peaks are consistent with literature reports.[17,19,20,36,46−48] The relative lattice parameters a and b are 1.6 and 0.38 nm, respectively. In comparison with the solution-processed RR-P3HT thin film, the $\pi-\pi$ stacking (010) diffraction peak of the RR-P3HT nanotubes has a stronger intensity, which is mainly attributed to the phenomenon that solution-processed RR-P3HT films prefer edge-on chain orientation on substrates.[36] In addition, the individual RR-P3HT nanotubes inside the template have significantly higher intensity than that of the RR-P3HT nanotube strands on the amorphous silicon at the (010) diffraction peak. At the same time, the intensities of the (100), (200), and (300) diffraction peaks of the individual RR-P3HT nanotubes show significant decrement comparing with the same diffraction peaks of the RR-P3HT nanotube strands. The decrease of the (100) and (200) diffraction peaks and increase of the (010) diffraction peak indicate strong anisotropic chain orientation in the RR-P3HT nanotubes. The crystallinity of a whole RR-P3HT nanotube was investigated and compared with RR-P3HT powders using WAXD, as shown in Figure S2. By normalizing the (100) peak, the (200), (300), and (010) peaks showed different peak intensity.[52] The intensities of the (200) and (300) diffraction peaks of the RR-P3HT powders are higher than the same diffraction peaks of the RR-P3HT nanotubes in AAO. The significant difference is the (010) diffraction peak of the RR-P3HT nanotube in AAO, which is clearly higher than the same diffraction peaks of the RR-P3HT powders. The significant difference between diffraction peak intensities presents the anisotropy of the RR-P3HT crystal in the entire nanotube. Based on the GIXRD and WAXD results, the anisotropy of RR-P3HT could form during the wetting process. To confirm the accuracy of our GIXRD and WAXD results, we further characterized the anisotropy of the RR-P3HT nanotubes using polarized photoluminescence (PL). In the polarized PL measurement, the RR-P3HT nanotubes were excited with a 490 nm wavelength. The corresponding results are shown in Figure 3b, and the setup of the polarized PL measurement is presented in Figure S3. The polarized emission peak maximum located at 645 nm for red shifts in the parallel direction is around 20 to 665 nm compared with the emission in the perpendicular direction with respect to the RR-P3HT nanotube axis. The perpendicular emission intensities (I_{HH} and I_{VH}) are much higher compared with those of the parallel emission intensities (I_{VV}), and the PL polarization ratio (I_{HH}/I_{VV}) is about 9.5, as shown in Figure 3b. The polarized parallel light excited the nanotubes to emit higher light intensity in the direction perpendicular to the RR-P3HT nanotubes. The different intensities of the emission light indicate the luminescence anisotropy of the RR-P3HT nanotubes, and this is consistent with the results of the GIXRD and WAXD measurements.

The above GIXRD, WAXD, and PL results confirm that a polymer melt wetting technique enables the preparation of the anisotropic RR-P3HT nanotubes, leading to an improved field-effect performance. In fact, the anisotropy of a polymer in nanochannels of the AAO template has been reported by studies,[11,27,31−33,49] and the chain orientation or crystallinity of the polymer in the spatial confinement is significantly different with that of the bulk polymer. Under capillary force, the polymer melt with low surface energy is absorbed into the nanochannels of the AAO template that has higher surface energy.[26] During the cooling processes of the polymer melts, the polymer chain orients itself perpendicular to the nanochannels.[27,31,49] The unique orientation of the polymer molecules is mainly attributed to the kinetic selection of the crystal growth process, which allows the lamellae to grow in the ⟨$hk0$⟩ direction parallel to the pore of the template along the nanochannels.[27] For RR-P3HT melt wetting, the RR-P3HT lamellae prefer to grow into the nanochannels in the ⟨$hk0$⟩ direction, which leads to the anisotropy of the as-prepared RR-P3HT nanotubes. As observed from the GIXRD, WAXD, and polarized PL results, the (010) diffraction peak of the individual RR-P3HT nanotubes and the emission intensity perpendicular to the RR-P3HT nanotubes are greatly enhanced. At the same time, the ⟨$h00$⟩ diffraction peak and the emission intensity decrease in the direction parallel to the RR-P3HT nanotubes. The luminescence anisotropy in the RR-P3HT nanotubes is mainly influenced by the orientation/alignment of the RR-P3HT chains to the polarized excitation light. Various

chromophore lengths exist in the RR-P3HT nanotubes because of conformational disorders. Hence, emissive excitons created on shorter segments may migrate to longer conjugated RR-P3HT segments that have lower energy and emit longer wavelength light. The transition dipole moments of the emission for most of the conjugated polymers prefer to move along the polymer chain. The increment of the emission intensity in the direction perpendicular to the RR-P3HT nanotubes indicates that the RR-P3HT chains prefer to be perpendicular to the nanotube axis. The (010) diffraction peak represents the face-on conformation[26] of the RR-P3HT lamellae, indicating that $\pi-\pi$ stacking formed by the thiophene ring of RR-P3HT prefers to be along the RR-P3HT nanotubes. The FET based on such a single RR-P3HT nanotube has higher carrier mobility compared with the solution-processed RR-P3HT thin film FET because of the preferred orientation of the RR-P3HT chain and lamella. The increment of the carrier mobility further confirms the preferred orientation of the RR-P3HT chain and lamella.

The wetting behavior of the polymer melt in the nanochannel is influenced by thermal properties of the polymer. Thus, we performed the DSC measurement to investigate the thermal properties of RR-P3HT. The DSC curves of bulk RR-P3HT are shown in Figure 4 and are used to determine the

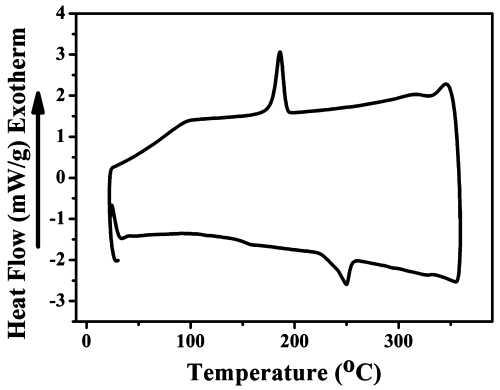

Figure 4. DSC curves of bulk RR-P3HT.

wetting temperature of the polymer melts. As shown in Figure 4, the glass transition temperature, melting point, and crystallization temperature of bulk RR-P3HT are 158, 250, and 180 °C, respectively. Therefore, the wetting temperatures were set between 200 and 250 °C (melting point). During the wetting process, the RR-P3HT melts with low surface energy were absorbed into the nanochannels of the AAO templates. The ordering of the polymer chains and, eventually, the crystallization occurred during the cooling of melts. The cooling rate is important, as it significantly affects the crystallization and polymer chain orientation of the nanowires/nanotubes.[28] In this study, the cooling rate was set at 10−15 °C/min.

Figures 5a-d show the SEM images of the typical cross-section and top-view of the RR-P3HT nanotubes after removing AAO. The average diameter of the as-fabricated RR-P3HT nanotubes is around 200 nm, which is consistent with the through-hole channel diameter of the AAO template (shown in Figure S4, Supporting Information). As the diameter of the nanochannels of AAO is fixed at around 200 nm, the aspect ratio mainly depends on the length of the RR-P3HT nanotube, which is equal to the displacement length of RR-P3HT melts in AAO measured by SEM (Figures 5a-d).[37,38,50] The aspect-ratio tunability of the RR-P3HT nanotubes was investigated by changing the melt wetting temperature and time. The results are shown in Figures 5 e-f. As shown in Figures 5a and 5b, the RR-P3HT nanotubes at a wetting temperature of 210 °C and wetting time of 10 min exhibited a length of ∼6 μm and a relatively low aspect ratio of ∼25. Figure 5b represents the RR-P3HT nanostructures with a feature being consistent with the previously reported nanotubes fabricated using a polymer melt wetting technique.[26,48,51−58] Figures 5c and 5d show the RR-P3HT nanotubes fabricated at a wetting temperature of 250 °C and a wetting time of 10 min that exhibit a length of ∼60 μm and a substantially larger aspect ratio of ∼300 (Figure 5c). As shown in Figure 5c, the cone-like bundles consist of irregular polygons. This may be attributed to the collapse of the RR-P3HT nanotubes with a higher aspect ratio (∼300) because of the intrinsic self-attraction between the RR-P3HT nanotubes through van der Waals interaction[59] and the hydrostatic dilation stress, which occurred during the removal of AAO, water, and ethanol. Figure 5e shows the relationship between the displacement lengths of the RR-P3HT nanotubes in the AAO nanochannels and wetting temperatures at a wetting time of 10 min. The results indicate that the displacement lengths of the RR-P3HT nanotubes significantly increase with the increase in wetting temperature. In addition, a longer wetting time dramatically increases the displacement length of RR-P3HT melts in the nanochannels of AAO, as shown in Figure 5f. These results show similar trends with other polymers and are consistent with our previous results.[37,38]

The aspect ratio of the RR-P3HT nanotubes is mainly related to the diameter and length of the nanotubes. By controlling the anodization parameter, AAO with nanochannels with a broad range of diameter has been fabricated[53] and commercialized. The length of the RR-P3HT nanotubes is controlled by the wetting behavior of polymer melts, which could be investigated via the surface tension and viscosity of the polymer melts, and the size of the nanochannels of AAO. This could be understood by following the Lucas-Washburn equation,[60] $dz/dt = (R\gamma\cos\theta)/(4\eta z)$, where z is the displacement length of polymer melts in nanochannels, t is the wetting time of polymer melts, η is the viscosity of polymer melts, R is the hydraulic radius (diameter of nanochannel), γ is the surface tension, and θ is the contact angle. As shown in Figure 5e, the displacement length of the RR-P3HT nanotubes significantly increases with increasing temperature from 200 to 250 °C. This shows that a decrease in the viscosity of the RR-P3HT melts with the elevated temperature has an important role in the wetting behavior of RR-P3HT melts. As shown in Figure 5f, prolonged wetting time increases the displacement length. Through controlling wetting temperature and time, the length of the RR-P3HT nanotubes could be tuned from 3 to 60 μm. The formation of the RR-P3HT nanotubes at all the wetting temperatures would be attributed to the complete wetting of precursor melts in the nanochannel. The wetting transition temperature of the partial to complete wetting have not been observed because of two factors, namely, the high wetting temperature (200 °C, which is about 50 °C above the Tg of RR-P3HT) and the relative low molecular weight (Mn is 54 000−75 000 with M_w/M_n, less than 2.5). The RR-P3HT with relatively low molecular weight would preferentially wet the nanochannel of AAO at a high wetting temperature. The as-prepared arrays and cone-bundles show potential applications in polymer solar cells[4] and chemical sensors.[12] Therefore, a polymer melt wetting technique enables

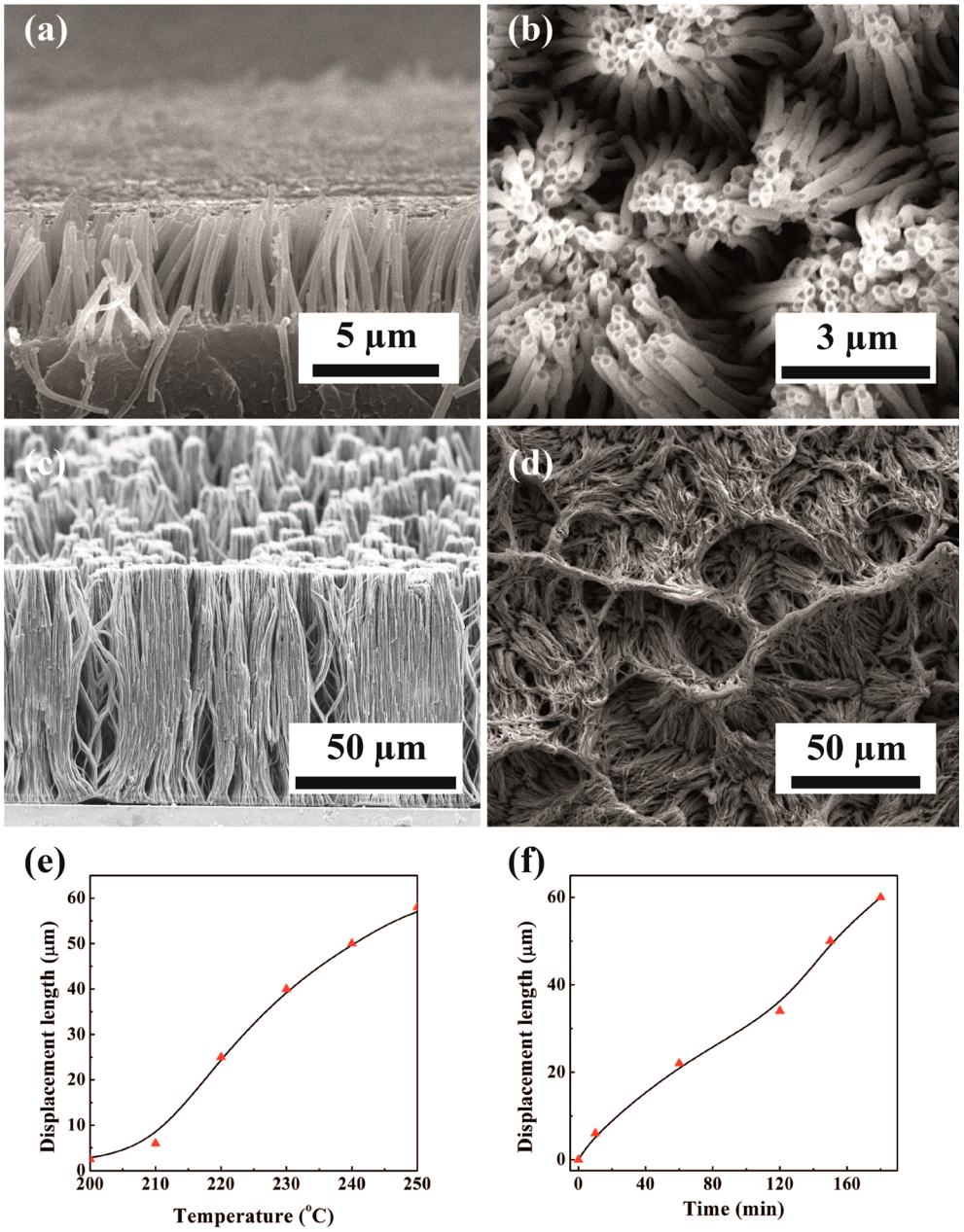

Figure 5. SEM images of (a) cross-section and (b) top-view of the RR-P3HT nanotubes fabricated at a wetting temperature of 210 °C with a wetting time of 10 min; (c) cross-section and (d) top-view of the RR-P3HT nanotubes fabricated at a wetting temperature of 250 °C with a wetting time of 10 min; and relationship between displacement length of RR-P3HT in nanochannels with wetting (e) temperature and (f) time.

the preparation of the highly anisotropic semiconducting polymer nanowires/nanotubes with tunable aspect ratios and diameters, which have a wide variety of potential applications.[54,61,62]

CONCLUSIONS

RR-P3HT nanotubes with a diameter of around 200 nm and aspect ratios from 15 to 300 were successfully fabricated using a polymer melt wetting technique. The aspect ratios of the RR-P3HT nanotubes were tuned by controlling wetting the temperature and time. FET devices based on a single RR-P3HT nanotube showed carrier mobility of 0.14 ± 0.02 $cm^2/V·s$. Results of GIXRD and polarized photoluminescence spectra indicated that the orientation of $\pi-\pi$ stacking of RR-P3HT was perpendicular to the RR-P3HT nanotubes. The crystalline nanotubes prepared by such a polymer melt wetting technique could be used in various electronic and optoelectronic devices, such as LEDs, solar cells, nanoscale lasers, memory devices, photo switches, ion batteries, and vapor sensors.

ASSOCIATED CONTENT

Supporting Information

Detailed information on WAXD and polarized photoluminescence spectra. This material is available free of charge via the Internet at http://pubs.acs.org.

AUTHOR INFORMATION

Corresponding Author

*Phone: 852 3442 2729. E-mail: val.roy@cityu.edu.hk.

Funding

The authors are grateful to strategic research grant 7003041 of the City University of Hong Kong and to the Research Grants Council of the Hong Kong Special Administrative Region (Project No. T23-713/11) and the Natural Science for Youth Foundation (Project No. 21303081) for providing financial support.

Notes

The authors declare no competing financial interest.

■ ACKNOWLEDGMENTS

We acknowledge grants from the innovation of science and Technology Committee of Shenzhen (JCYJ20120618115445056) and the Research Grants Council of the Hong Kong Special Administrative Region (Project No.T23-713/11). The authors are grateful to Mr. T. F. Hung for providing technical support.

■ REFERENCES

(1) Wang, W.; Lu, X.; Li, Z.; Lei, J.; Liu, X.; Wang, Z.; Zhang, H.; Wang, C. One-Dimensional Polyelectrolyte/Polymeric Semiconductor Core/Shell Structure: Sulfonated Poly(arylene ether ketone)/Polyaniline Nanofibers for Organic Field-Effect Transistors. *Adv. Mater.* **2011**, *23*, 5109−5112.

(2) Zheng, G. F.; Lu, W.; Jin, S.; Lieber, C. M. Synthesis and Fabrication of High-performance n-type Silicon Nanowire Transistors. *Adv. Mater.* **2004**, *16*, 1890−1893.

(3) Vohra, V.; Giovanella, U.; Tubino, R.; Murata, H.; Botta, C. Electroluminescence from Conjugated Polymer Electrospun Nanofibers in Solution Processable Organic Light-Emitting Diodes. *ACS Nano* **2011**, *5*, 5572−5578.

(4) Hochbaum, A. I.; Yang, P. Semiconductor Nanowires for Energy Conversion. *Chem. Rev.* **2010**, *110*, 527−546.

(5) Berson, S.; De Bettignies, R.; Bailly, S.; Guillerez, S. Poly (3-hexylthiophene) Fibers for Photovoltaic Applications. *Adv. Funct. Mater.* **2007**, *17*, 1377−1384.

(6) Kim, J. S.; Lee, J. H.; Park, J. H.; Shim, C.; Sim, M.; Cho, K. High-efficiency Organic Solar Cells Based on Preformed Poly (3-hexylthiophene) Nanowires. *Adv. Funct. Mater.* **2011**, *21*, 480−486.

(7) Scofield, A. C.; Kim, S. H.; Shapiro, J. N.; Lin, A.; Liang, B. L.; Scherer, A.; Huffaker, D. L. Bottom-up Photonic Crystal Lasers. *Nano Lett.* **2011**, *11*, 5387−5390.

(8) White, S. I.; Vora, P. M.; Kikkawa, J. M.; Winey, K. I. Resistive Switching in Bulk Silver Nanowire-Polystyrene Composites. *Adv. Funct. Mater.* **2011**, *21*, 233−240.

(9) Di Benedetto, F.; Mele, E.; Camposeo, A.; Athanassiou, A.; Cingolani, R.; Pisignano, D. Photoswitchable Organic Nanofibers. *Adv. Mater.* **2008**, *20*, 314−318.

(10) Hwang, T. H.; Lee, Y. M.; Kong, B.-S.; Seo, J.-S.; Choi, J. W. Electrospun Core-Shell Fibers for Robust Silicon Nanoparticle-Based Lithium Ion Battery Anodes. *Nano Lett.* **2012**, *12*, 802−807.

(11) Li, M.; Wu, H.; Huang, Y.; Su, Z. H. Effects of Temperature and Template Surface on Crystallization of Syndiotactic Polystyrene in Cylindrical Nanopores. *Macromolecules* **2012**, *45*, 5196−5200.

(12) Li, D.; Huang, J.; Kaner, R. B. Polyaniline Nanofibers: A Unique Polymer Nanostructure for Versatile Applications. *Acc. Chem. Res.* **2009**, *42*, 135−145.

(13) McAlpine, M. C.; Ahmad, H.; Wang, D.; Heath, J. R. Highly Ordered Nanowire Arrays on Plastic Substrates for Ultrasensitive Flexible Chemical Sensors. *Nat. Mater.* **2007**, *6*, 379−384.

(14) Park, D. H.; Kim, N.; Cui, C.; Hong, Y. K.; Kim, M. S.; Yang, D.-H.; Kim, D.-C.; Lee, H.; Kim, J.; Ahn, D. J.; Joo, J. DNA Detection Using a Light-emitting Polymer Single Nanowire. *Chem. Commun.* **2011**, *47*, 7944−7946.

(15) Kim, F. S.; Guo, X.; Watson, M. D.; Jenekhe, S. A. High-Mobility Ambipolar Transistors and High-Gain Inverters from a Donor-Acceptor Copolymer Semiconductor. *Adv. Mater.* **2010**, *22*, 478−482.

(16) Yang, H.; Shin, T. J.; Bao, Z.; Ryu, C. Y. Structural Transitions of Nanocrystalline Domains in Regioregular Poly(3-hexyl thiophene) Thin Films. *J. Polym. Sci., Part B: Polym. Phys.* **2007**, *45*, 1303−1312.

(17) Aiyar, A. R.; Hong, J.-I.; Nambiar, R.; Collard, D. M.; Reichmanis, E. Tunable Crystallinity in Regioregular Poly(3-Hexylthiophene) Thin Films and Its Impact on Field Effect Mobility. *Adv. Funct. Mater.* **2011**, *21*, 2652−2659.

(18) Brinkmann, M. Structure and Morphology Control in Thin Films of Regioregular Poly(3-hexylthiophene). *J. Polym. Sci., Part B: Polym. Phys.* **2011**, *49*, 1218−1233.

(19) Zen, A.; Saphiannikova, M.; Neher, D.; Grenzer, J.; Grigorian, S.; Pietsch, U.; Asawapirom, U.; Janietz, S.; Scherf, U.; Lieberwirth, I.; Wegner, G. Effect of Molecular Weight on the Structure and Crystallinity of Poly(3-hexylthiophene). *Macromolecules* **2006**, *39*, 2162−2171.

(20) Yang, H. C.; Shin, T. J.; Yang, L.; Cho, K.; Ryu, C. Y.; Bao, Z. N. Effect of Mesoscale Crystalline Structure on the Field-Effect Mobility of Regioregular Poly(3-hexyl thiophene) in Thin-film Transistors. *Adv. Funct. Mater.* **2005**, *15*, 671−676.

(21) Huang, Y.; Cheng, H.; Han, C. C. Temperature Induced Structure Evolution of Regioregular Poly(3-hexylthiophene) in Dilute Solution and its Influence on Thin Film Morphology. *Macromolecules* **2010**, *43*, 10031−10037.

(22) Di Benedetto, F.; Camposeo, A.; Pagliara, S.; Mele, E.; Persano, L.; Stabile, R.; Cingolani, R.; Pisignano, D. Patterning of Light-emitting Conjugated Polymer Nanofibres. *Nat. Nanotechnol.* **2008**, *3*, 614−619.

(23) Liu, H. Q.; Reccius, C. H.; Craighead, H. G. Single Electrospun Regioregular Poly(3-hexylthiophene) Nanofiber Field-Effect Transistor. *Appl. Phys. Lett.* **2005**, *87*, 253106.

(24) Li, D.; Babel, A.; Jenekhe, S. A.; Xia, Y. N. Nanofibers of Conjugated Polymers Prepared by Electrospinning with a Two-capillary Spinneret. *Adv. Mater.* **2004**, *16*, 2062−2066.

(25) Brinkmann, M.; Wittmann, J. C. Orientation of Regioregular Poly(3-hexylthiophene) by Directional Solidification: A Simple Method to Reveal the Semicrystalline Structure of A Conjugated Polymer. *Adv. Mater.* **2006**, *18*, 860−863.

(26) Steinhart, M.; Wendorff, J. H.; Greiner, A.; Wehrspohn, R. B.; Nielsch, K.; Schilling, J.; Choi, J.; Gosele, U. Polymer Nanotubes by Wetting of Ordered Porous Templates. *Science* **2002**, *296*, 1997−1997.

(27) Steinhart, M.; Goring, P.; Dernaika, H.; Prabhukaran, M.; Gosele, U.; Hempel, E.; Thurn-Albrecht, T. Coherent Kinetic Control Over Crystal Orientation in Macroscopic Ensembles of Polymer Nanorods and Nanotubes. *Phys. Rev. Lett.* **2006**, *97*, 027801.

(28) Maiz, J.; Martin, J.; Mijangos, C. Confinement Effects on the Crystallization of Poly(ethylene oxide) Nanotubes. *Langmuir* **2012**, *28*, 12296−12303.

(29) Nakagawa, S.; Kadena, K.; Ishizone, T.; Nojima, S.; Shimizu, T.; Yamaguchi, K.; Nakahama, S. Crystallization Behavior and Crystal Orientation of Poly(epsilon-caprolactone) Homopolymers Confined in Nanocylinders: Effects of Nanocylinder Dimension. *Macromolecules* **2012**, *45*, 1892−1900.

(30) Martin, J.; Mijangos, C. Tailored Polymer-Based Nanofibers and Nanotubes by Means of Different Infiltration Methods into Alumina Nanopores. *Langmuir* **2009**, *25*, 1181−1187.

(31) Steinhart, M.; Senz, S.; Wehrspohn, R. B.; Gosele, U.; Wendorff, J. H. Curvature-directed Crystallization of Poly(vinylidene difluoride) in Nanotube Walls. *Macromolecules* **2003**, *36*, 3646−3651.

(32) Wu, H.; Wang, W.; Yang, H. X.; Su, Z. H. Crystallization and Orientation of Syndiotactic Polystyrene in Nanorods. *Macromolecules* **2007**, *40*, 4244−4249.

(33) Wu, H.; Wang, W.; Huang, Y.; Wang, C.; So, Z. H. Polymorphic Behavior of Syndiotactic Polystyrene Crystallized in Cylindrical Nanopores. *Macromolecules* **2008**, *41*, 7755−7758.

(34) Santos, A.; Formentin, P.; Pallares, J.; Ferre-Borrull, J.; Marsal, L. F. Quasi-ordered P3HT Nanopillar-nanocap Structures with Controlled Size. *Mater. Lett.* **2010**, *64*, 371−374.

(35) Baek, S.; Park, J. B.; Lee, W.; Han, S.-H.; Lee, J.; Lee, S.-H. A Facile Method to Prepare Regioregular Poly(3-hexylthiophene) Nanorod Arrays Using Anodic Aluminium Oxide Templates and Capillary Force. *New J. Chem.* **2009**, *33*, 986−990.
(36) Sirringhaus, H.; Brown, P. J.; Friend, R. H.; Nielsen, M. M.; Bechgaard, K.; Langeveld-Voss, B. M. W.; Spiering, A. J. H.; Janssen, R. A. J.; Meijer, E. W.; Herwig, P.; de Leeuw, D. M. Two-Dimensional Charge Transport in Self-organized, High-mobility Conjugated Polymers. *Nature* **1999**, *401*, 685−688.
(37) Tian, W.; Yung, K. L.; Xu, Y.; Huang, L.; Kong, J.; Xie, Y. Enhanced Nanoflow Behaviors of Polymer Melts Using Dispersed Nanoparticles and Ultrasonic Vibration. *Nanoscale* **2011**, *3*, 4094−4100.
(38) Tian, W.; Xu, Y.; Huang, L.; Yung, K.-L.; Xie, Y.; Chen, W. [Small beta]-Cyclodextrin and Its Hyperbranched Polymers-induced Micro/nanopatterns and Tunable Wettability on Polymer surfaces. *Nanoscale* **2011**, *3*, 5147−5155.
(39) Liu, Y.; Li, B.; Wu, X.; Cong, Y. Effect of Organic Modification on Oxygen Sensing Properties of Xerogel with a Covalently Linked Ruthenium(II) Complex. *J. Optoelectron. Adv. Mater.* **2009**, *11*, 880−886.
(40) Perlich, J.; Rubeck, J.; Botta, S.; Gehrke, R.; Roth, S. V.; Ruderer, M. A.; Prams, S. M.; Rawolle, M.; Zhong, Q.; Körstgens, V.; Müller-Buschbaum, P. Grazing incidence wide angle x-ray scattering at the wiggler beamline BW4 of HASYLAB. *Rev. Sci. Instrum.* **2010**, *81*, 105105.
(41) Sanandajia, N.; Ovaskainena, L.; Klein Gunnewiekb, M.; Vancsob, G. J.; Hedenqvista, M. S.; Yuc, S.; Erikssond, L.; Rothc, S. V.; Geddea, U. W. Unusual crystals of poly(ε-caprolactone) by unusual crystallisation: The effects of rapid cooling and fast solvent loss on the morphology, crystal structure and melting. *Polymer* **2013**, *54*, 1497−1503.
(42) Lee, S.; Moon, G. D.; Jeong, U. Continuous Production of Uniform Poly(3-hexylthiophene) (P3HT) Nanofibers by Electrospinning and Their Electrical Properties. *J. Mater. Chem.* **2009**, *19*, 743−748.
(43) Chen, J.-Y.; Kuo, C.-C.; Lai, C.-S.; Chen, W.-C.; Chen, H.-L. Manipulation on the Morphology and Electrical Properties of Aligned Electrospun Nanofibers of Poly(3-hexylthiophene) for Field-Effect Transistor Applications. *Macromolecules* **2011**, *44*, 2883−2892.
(44) Byun, J.; Kim, Y.; Jeon, G.; Kim, J. K. Array of Free-Standing Poly(3-hexylthiophene) Nanotubes on Conducting Substrates via Solution Wetting. *Macromolecules* **2011**, *44*, 8558−8562.
(45) Kim, D.; Park, Y.; Jang, Y.; Yang, H.; Kim, Y. H.; Han, J.; Moon, D.; Park, S.; Chang, T.; Chang, C. Enhancement of Field-Effect Mobility Due to Surface-Mediated Molecular Ordering in Regioregular Polythiophene Thin Film Transistors. *Adv. Funct. Mater.* **2005**, *15*, 77−82.
(46) Yang, H.; LeFevre, S. W.; Ryu, C. Y.; Bao, Z. Solubility-driven Thin Film Structures of Regioregular Poly(3-hexyl thiophene) Using Volatile Solvents. *Appl. Phys. Lett.* **2007**, *90*, 172116.
(47) Wu, Z.; Petzold, A.; Henze, T.; Thurn-Albrecht, T.; Lohwasser, R. H.; Sommer, M.; Thelakkat, M. Polymorphic Behavior of Syndiotactic Polystyrene Crystallized in Cylindrical Nanopores. *Macromolecules* **2010**, *43*, 4646−4653.
(48) Lilliu, S.; Agostinelli, T.; Pires, E.; Hampton, M.; Nelson, J.; Macdonald, J. E. Dynamics of Crystallization and Disorder during Annealing of P3HT/PCBM Bulk Heterojunctions. *Macromolecules* **2011**, *44*, 2725−2734.
(49) Shin, K.; Woo, E.; Jeong, Y. G.; Kim, C.; Huh, J.; Kim, K. W. Crystalline Structures, Melting, and Crystallization of Linear Polyethylene in Cylindrical Nanopores. *Macromolecules* **2007**, *40*, 6617−6623.
(50) Yung, K.-L.; Kong, J.; Xu, Y. Studies On Flow Behaviors of Polymer Melts in Nanochannels by Wetting Actions. *Polymer* **2007**, *48*, 7645−7652.
(51) Pulamagatta, B.; Yau, M.; Gunkel, I.; Thurn-Albrecht, T.; Schröter, K.; Pfefferkorn, D.; Kressler, J.; Steinhart, M.; Binder, W. Block Copolymer Nanotubes by Melt-infiltration of Nanoporous Aluminum Oxide. *Adv. Mater.* **2011**, *23*, 781−786.
(52) Steinhart, M.; Göring, P.; Dernaika, H.; Prabhukaran, M.; Gösele, U.; Hempel, E.; Thurn-Albrecht, T. Coherent Kinetic Control over Crystal Orientation in Macroscopic Ensembles of Polymer Nanorods and Nanotubes. *Phys. Rev. Lett.* **2006**, *97*, 27801.
(53) Lee, W.; Ji, R.; Gosele, U.; Nielsch, K. Fast Fabrication of Long-range Ordered Porous Alumina Membranes by Hard Anodization. *Nat. Mater.* **2006**, *5*, 741−747.
(54) Yin, Z. G.; Zheng, Q. D. Controlled Synthesis and Energy Applications of One-Dimensional Conducting Polymer Nanostructures: An Overview. *Adv. Energy Mater.* **2012**, *2*, 179−218.
(55) She, X.; Song, G.; Li, J.; Han, P.; Yang, S.; Shulong, W.; Peng, Z. Non-Polar Polymer Nanotubes and Nanowires Fabricated by Wetting Anodic Aluminium Oxide Template. *Polym. J.* **2006**, *38*, 639−642.
(56) Kriha, O.; Zhao, L.; Pippel, E.; Gösele, U.; Wehrspohn, R. B.; Wendorff, J. H.; Steinhart, M.; Greiner, A. Organic Tube/Rod Hybrid Nanofibers with Adjustable Segment Lengths by Bidirectional Template Wetting. *Adv. Funct. Mater.* **2007**, *17*, 1327−1332.
(57) Jaime, M.; Jon, M.; Javier, S.; Carmen, M. Tailored Polymer-based Nanorods and Nanotubes by "Template synthesis": From Preparation to Applications. *Polymer* **2012**, *53*, 1149−1166.
(58) Zhang, M.; Dobriyal, P.; Chen, J.-T.; Russell, T.; Olmo, J.; Merry, A. Wetting Transition in Cylindrical Alumina Nanopores with Polymer Melts. *Nano Lett.* **2006**, *6*, 1075−1079.
(59) Girifalco, L. A.; Hodak, M.; Lee, R. S. Carbon Nanotubes, Buckyballs, Ropes, and a Universal Graphitic Potential. *Phys. Rev. B: Condens. Matter Mater. Phys.* **2000**, *62*, 13104−13110.
(60) Kim, E.; Xia, Y. N.; Whitesides, G. M. Polymer Microstructures Formed by Molding in Capillaries. *Nature* **1995**, *376*, 581−584.
(61) Schaffer, C. J.; Palumbiny, C. M.; Niedermeier, M. A.; Jendrzejewski, C.; Santoro, G.; Roth, S. V.; Muller-Buschbaum, P. A Direct Evidence of Morphological Degradation on a Nanometer Scale in Polymer Solar Cells. *Adv. Mater.* **2013**, *25*, 6760−6764.
(62) Sepe, A.; Rong, Z.; Sommer, M.; Vaynzof, Y.; Sheng, X.; Muller-Buschbaum, P.; Smilgies, D.-M.; Tan, Z.-K.; Yang, L.; Friend, R. H.; Steiner, U.; Huttner, S. Structure formation in P3HT/F8TBT blends. *Energy Environ. Sci.* **2014**, *7*, 1725−1736.